THE JOURNAL OF BIOLOGICAL CHEMISTRY VOL. 291, NO. 7, pp. 3423–3438, February 12, 2016

Munc13-4 Is a Rab11-binding Protein That Regulates Rab11-positive Vesicle Trafficking and Docking at the Plasma Membrane*[S]

Received for publication, November 23, 2015, and in revised form, December 2, 2015 Published, JBC Papers in Press, December 4, 2015, DOI 10.1074/jbc.M115.705871

Jennifer L. Johnson[‡], Jing He[‡], Mahalakshmi Ramadass[‡1], Kersi Pestonjamasp[§], William B. Kiosses[¶], Jinzhong Zhang[‡2], and Sergio D. Catz[‡3]

From the [‡]Department of Molecular and Experimental Medicine and [¶]Light Microscopy Core Facility, The Scripps Research Institute, La Jolla, California 92037 and [§]Cancer Center Microscopy Shared Resource, University of California San Diego, La Jolla, California 92093

The small GTPase Rab11 and its effectors control trafficking of recycling endosomes, receptor replenishment and the up-regulation of adhesion and adaptor molecules at the plasma membrane. Despite recent advances in the understanding of Rab11-regulated mechanisms, the final steps mediating docking and fusion of Rab11-positive vesicles at the plasma membrane are not fully understood. Munc13-4 is a docking factor proposed to regulate fusion through interactions with SNAREs. In hematopoietic cells, including neutrophils, Munc13-4 regulates exocytosis in a Rab27a-dependent manner, but its possible regulation of other GTPases has not been explored in detail. Here, we show that Munc13-4 binds to Rab11 and regulates the trafficking of Rab11-containing vesicles. Using a novel Time-resolved Fluorescence Resonance Energy Transfer (TR-FRET) assay, we demonstrate that Munc13-4 binds to Rab11a but not to dominant negative Rab11a. Immunoprecipitation analysis confirmed the specificity of the interaction between Munc13-4 and Rab11, and super-resolution microscopy studies support the interaction of endogenous Munc13-4 with Rab11 at the single molecule level in neutrophils. Vesicular dynamic analysis shows the common spatio-temporal distribution of Munc13-4 and Rab11, while expression of a calcium binding-deficient mutant of Munc13-4 significantly affected Rab11 trafficking. Munc13-4-deficient neutrophils showed normal endocytosis, but the trafficking, up-regulation, and retention of Rab11-positive vesicles at the plasma membrane was significantly impaired. This correlated with deficient NADPH oxidase activation at the plasma membrane in response to Rab11 interference. Our data demonstrate that Munc13-4 is a Rab11-binding partner that regulates the final steps of Rab11-positive vesicle docking at the plasma membrane.

Rab GTPases are membrane organizers that regulate the specificity of subcellular compartments and trafficking of these compartments through interactions with specific effectors (1). In particular, Rab11, a ubiquitously expressed GTPase, has been implicated in the regulation of several intracellular mechanisms including recycling endosome trafficking, transport of cargo from the sorting endosomes and the trans-Golgi network to the endosomal recycling compartment and regulation of trafficking during cytokinesis (2). In addition, the Rab11 family of GTPases, comprised by Rab11a, Rab11b and Rab11c/Rab25, are known to regulate several cellular functions including exocytosis (3), phagocytosis (4), and cell-cell communication (5). Rab11 functions are regulated by a broad range of molecular interactors and effectors (2), and proteomic analyses have identified a large array of structurally diverse molecules that interact with Rab11. The most studied family of Rab11 effectors, FIPs (Rab11 family-interacting proteins),[4] comprises five members. Rip11, FIP2, and RCP are characterized by the presence of a conserved Rab11-binding domain at their C terminus and a C2 domain at their N terminus, and FIP3 and FIP4 are characterized by the presence of EF-hand domains but lack C2 domains (extensively reviewed in Ref. 6). Despite the increasing knowledge in the function of Rab11 and effectors in the regulation of cellular processes, it is accepted that the mechanism of Rab11 recruitment to specific sets of membranes and the possible cross-regulation of Rab11 functions by multiple effectors require further investigation (2). In particular, although both the mobilization of recycling endosomes and exocytosis would require the ultimate fusion of Rab11-containg vesicles with the plasma membrane, the molecular mechanisms regulating these processes remain elusive, and the Rab11 effectors mediating fusion are not fully identified.

Munc13-4 is a 120-kDa factor expressed in several cells and tissues with secretory functions. It is characterized by the presence of two C2-domains at the N and C terminus and two central Munc-homology domains (MHC) (7). The importance of these domains in the interaction of Munc13-4 with SNARE proteins to mediate membrane fusion has been recently described (8), and Munc13-4 is considered a regulator of vesicle tethering and membrane fusion (9). Several studies have shown

* This work was supported by U.S. Public Health Service Grants HL088256 and GM105894 (to S. D. C.). The authors declare that they have no conflicts of interest with the contents of this article. The content is solely the responsibility of the authors and does not necessarily represent the official views of the National Institutes of Health.
[S] This article contains supplemental movies S1–S4.
[1] Postdoctoral fellow from the AHA Western State Affiliates.
[2] Postdoctoral fellow of the Cystinosis Research Foundation.
[3] To whom correspondence should be addressed. Tel.: (858)-784-7932; Fax: (858)-784-2054; E-mail: scatz@scripps.edu.

[4] The abbreviations used are: FIP, family-interacting protein; MHC, Munc-homology domain; TR-FRET, time-resolved fluorescence resonance energy transfer; GTPγS, guanosine 5′-3-*O*-(thio)triphosphate; TIRFM, total internal reflection fluorescence microscopy; LPS, lipopolysaccharide; SLO, streptolysin-O.

that Munc13-4 is an essential regulator of lytic granule exocytosis at the immunological synapse (10), neutrophil granule secretion (11, 12), and platelet-dense granule exocytosis (13). In fact, Munc13-4 deficiency is associated with the human severe immunodeficiency FHL3 caused by the inefficiency of immune cells to mediate killing of pathogens and infected cells (9). Based on the similarity of this phenotype with that observed in Rab27a-deficient patients along with pull-down studies, protein-protein interaction, and functional assays, Munc13-4 was identified as a Rab27a-specific effector (14). Despite shared roles in regulating common secretory pathways, Munc13-4 regulates many cellular functions in a Rab27a-independent manner including phagosomal maturation in neutrophils (15), the differential secretory response to stimuli in NK cells (16) and the regulation of readily releasable secretory granules in granulocytes (12). It is therefore unclear how these discrete molecular events during exocytosis are regulated by Munc13-4. In addition, although some of the molecular components that regulate Rab11-positive vesicle exocytosis have been identified (17), the mechanisms regulating the final steps of exocytosis of Rab11-containing vesicles and many of the molecular interactions mediating this process remain obscure. Here, using biochemical approaches, vesicular dynamic assays and super-resolution microscopy, we have identified Munc13-4 as a Rab11a binding protein. Furthermore, using analysis of vesicular dynamics and high resolution microscopy, we establish the functional association of Munc13-4 and Rab11 and demonstrate that Munc13-4 regulates the transport of Rab11a-containing vesicles and the association of Rab11-containing vesicles with the plasma membrane during exocytosis.

Experimental Procedures

Animals—C57BL/6 Munc13-4$^{jinx/jinx}$ mice (here referred to as *Jinx*) (18) and their parental strain, C57BL/6 (wild type) were used in this work. Mice (6–12 weeks old) were maintained in a pathogen-free environment and had access to food and water *ad libitum*. All animal studies were performed in compliance with the United States Department of Health and Human Services Guide for the Care and Use of Laboratory Animals. All studies were conducted according to National Institutes of Health and institutional guidelines and with approval from the animal review board at The Scripps Research Institute.

Expression Vectors and Mutagenesis—GFP-Rab11a, Rab11S25N, Rab11Q70L, Rab22a, Rab5, Rab7, and Rab34 were obtained from Addgene. mCherry-Munc13-4 and Flag-Munc13-4 were obtained from Genecopoeia. Munc13-4 mutagenesis was carried out using a QuikChange Site-directed Mutagenesis Kit (Agilent) following the manufacturer's instructions. The primers used for mutagenesis were: For the C2A domain: 5′-attctgggcaaaAatgtcagtgggttcagcAacccctactgcc-3′; 5′-ggcagtaggggtTgctgaacccactgacatTtttgcccagaat-3′. For the C2B domain: 5′- ctgctgcccctgAactccaatggctccagcAacccctttgtcc-3′; 5′-ggacaaaggggtTgctggagccattggagtTcaggggcagcag-3′.

Binding Assay—For time-resolved fluorescence resonance energy transfer binding assays (TR-FRET), 293T cell were transfected using Lipofectamine 2000 (Life Technologies) per the manufacturer's instructions. The cells were resuspended in Relaxation buffer (100 mM KCl, 3 mM NaCl, 3.5 mM $MgCl_2$, 1 mM ATP, and 10 mM PIPES (pH 7.3) containing Complete EGTA-free anti-protease mixture (Roche)). For lysis, we use nitrogen cavitation, a method that disrupts the plasma membrane but preserves intracellular organelles and minimizes lysosomal protease release (19). After lysis, lysates are spun down at 14,000 rpm for 1 min at 4 °C to remove nuclei and tested in small scale TR-FRET reactions, flash-frozen using liquid nitrogen, and subsequently stored at −80 °C for at least 8 months without detectable loss of activity. Protein expression was analyzed by Western blot as well as by fluorometry (EGFP) using an Envision plate reader. Lysates expressing Flag-tagged Munc13-4 and equimolar GFP-tagged Rab GTPases (~250 nM) were used to evaluate protein-protein interactions. The reactions were carried out in 384-well plates and started by addition of the Terbium cryptate-conjugated anti-Flag antibody (Cisbio) at 15 pg/μl in a final volume of 10 μl. The reactions were carried out at 21 °C, and the emission ratio of the acceptor (GFP, 520 nm)/donor (Tb, 490 nm) was followed for up to 30 min after the addition of antibody using a 2104 EnVision multilabel plate reader with high energy Time-Resolved Fluorescence laser excitation flash lamps to process 384-well plates.

For competition assays, GST-fusion proteins were purified in *Escherichia coli* as described previously (20) and extensively dialyzed against PBS. GST-Rab11 was loaded with GTPγS by incubation in loading buffer containing 15 mM final concentration of EDTA, followed by the addition of GTPγS to a final concentration of 0.2 mM and 15 min additional incubation at room temperature. The reactions were stopped by the addition of stop buffer to a final concentration of 60 mM $MgCl_2$. IC_{50} values were determined using lysates expressing 79 nM EGFP-Rab11, so that the concentration of EGFP-Rab11 was less than half the IC_{50}. K_d was then calculated using the homologous competitive binding curve fitted to a built-in equation of one-site competition (GraphPad Prism). The assay assumes that GST-Rab11 and EGFP-Rab11 have similar affinities for Munc13-4.

SDS-PAGE Western Blotting—Proteins were separated by gel electrophoresis using NuPAGE gels and MOPS buffer (Life Technologies). Proteins were transferred onto nitrocellulose membranes for 180 min at 70 V and 4 °C. The membranes were blocked with PBS containing 5% (*w*/*v*) blotting-grade nonfat dry milk blocker (Rockland) and 0.05% (*w*/*v*) Tween 20. Proteins were detected by probing the membranes with the indicated primary antibodies at appropriate dilutions and using a detection system consisting of horseradish peroxidase (HRP)-conjugated secondary antibodies (Bio-Rad) and the chemiluminescence substrates SuperSignal, WestPico, or WestFemto (Thermo Scientific), then visualized using Hyperfilm (Denville Scientific).

Immunoprecipitation—For the immunoprecipitation assay, cells were lysed by nitrogen cavitation in Relaxation buffer, the samples were cleared by centrifugation, and the supernatants were then incubated with anti-M2-agarose beads (Sigma) at 4 °C, rotating overnight. Following three washes with lysis buffer, the immunoprecipitates were subjected to Western blotting. For immunoprecipitation assays of endogenous proteins, human neutrophils were treated with the protease inhib-

itor diisopropylfluorophosphate (DFP), washed with 10 ml of Relaxation buffer containing Complete EGTA-free anti-protease mixture (Roche), and disrupted by nitrogen cavitation in Relaxation buffer. Next, cleared cell lysates (1000 μg of total protein) were rotated overnight at 4 °C with anti-Rab11 (Rabbit mAb(D4F5) or Rabbit (DA1E) mAb IgG isotype control antibodies (Cell Signaling Technologies) (1 μg) in a total volume of 500 μl. The samples were further incubated in the presence of 100 μl of protein A/G-conjugated magnetic beads (Pierce) for 1 h. The beads were washed three times in lysis buffer, once in distilled water, and magnetically isolated as described by the manufacturer (Pierce). The beads were resuspended in 100 μl of l× non-reducing sample buffer, heated at 95 °C for 10 min, and samples were analyzed by Western blot.

Mouse Neutrophil Isolation—Bone marrow-derived neutrophils were isolated using a Percoll gradient fractionation system as described (21). A three-layer Percoll gradient was used (52, 64, and 72%), neutrophils were isolated from the 64 to 72% interface, washed, and used in all the assays.

Immunofluorescence Analysis and Confocal Microscopy—Neutrophils were seeded on untreated coverglasses (Cole-Parmer) and incubated at 37 °C for 1 h, then fixed with 1.5% paraformaldehyde for 15 min, or with 4% PAF for 10 min, permeabilized with 0.02% saponin, and blocked with 1% BSA in PBS. Samples were labeled with the indicated primary antibodies overnight at 4 °C in the presence of 0.02% saponin and 1% BSA. Samples were washed and subsequently incubated with the appropriate combinations of Alexa Fluor (488, 594, or 633)-conjugated donkey anti-rabbit, anti-rat, anti-sheep, or anti-mouse secondary antibodies (Life Technologies). Samples were analyzed with a Zeiss LSM 710 laser scanning confocal microscope (LSCM) attached to a Zeiss Observer Z1 microscope at 21 °C, using a 63× oil Plan Apo, 1.4-numerical-aperture objective. Images were collected using ZEN-LSM software and processed using Image*J* and Adobe Photoshop CS4.

Nucleofection—Mouse neutrophil nucleofection was carried out using the Lonza 4D-Nucleofector X-unit system (Lonza) following the manufacturer's instruction. In brief, mouse neutrophils were counted, and 1 million cells were resuspended in 20 μl of Lonza P3 solution with 0.1–1 μg of DNA, the solutions were transferred into the X-unit, then subjected to nucleofection in the 4D-Nucleofector using program EA-100. The cells were then resuspended in phenol red-free RPMI (Life Technologies) and seeded into 4-chamber 35-mm glass bottom dishes (number 1.5 borosilicate coverglass, In Vitro Scientific). Cells were incubated at 37 °C for at least 4 h before microscopy analysis.

Total Internal Reflection Fluorescence (TIRF) Microscopy—TIRF microscopy experiments were performed using a 100× 1.45 numerical aperture TIRF objective (Nikon) on a Nikon TE2000U microscope custom modified with a TIRF illumination module as described (21). Images were acquired on a 14-bit, cooled charge-coupled device camera (Hamamatsu) controlled through NIS-Elements software. For live experiments, the images were recorded using 300–500 ms exposures depending on the fluorescence intensity of the sample. For the quantitative analysis of the fluorescence intensity of Rab11 in fixed cells, the exposure time and gain was maintained throughout the experiment to comparatively analyze unstimulated and stimulated wild type and Munc13-4-KO cells. The images were then analyzed using Image*J* software. To this end, the outline of the cells was selected using the "manual" tool, and the ratio of the fluorescence intensity/cell area was then calculated using the "measure" tool.

Super-resolution Microscopy—STORM was performed as described previously (22). Briefly, cells were labeled with anti-Munc13-4 and either anti-Rab11 or anti-Rab5 primary antibodies and Alexa-647- and Atto-488-conjugated secondary antibodies. Samples were suspended in freshly prepared STORM buffer (50 mM Tris, pH 8.0, 10 mM NaCl, 10% glucose, 0.1 M mercaptoethanolamine (Cysteamine Sigma-Aldrich), 56 units/ml glucose oxidase (from *Aspergillus niger*, Sigma-Aldrich), and 340 units/ml catalase (from bovine liver, Sigma-Aldrich)), and imaged on a Nikon Ti super-resolution microscope. Samples were imaged using a 100× 1.49 NA Apo TIRF objective either with or without TIRF illumination. Images were collected on an ANDOR IXON3 Ultra DU897 EMCCD camera using the multi-color continuous mode setting in the Nikon Elements software. Power on the 488 nm and 647 nm lasers was adjusted to enable collection of between 50 and 300 molecules per 256 × 256 camera pixel frames at appropriate threshold settings for each channel. Collection was stopped after a sufficient number of frames were collected (usually yielding 1–2 million molecules), and the super-resolution images were reconstructed with the Nikon STORM software.

The STORM technology used for the present study has been developed by the Xiaowei Zhuang laboratory at Harvard University (23) and licensed to Nikon. The position of individual molecules has been localized with high accuracy by switching them on and off sequentially using the 488 and 647 lasers at appropriate power settings. The positions determined from multiple switching cycles can show a substantial drift over the duration of the acquisition. This error is considerably reduced by calculating and correcting for sample drift over the course of the experiment by an auto-correlation method used by the Nikon software. This is done by correlating STORM images reconstructed from subsets of localizations at different time segments to that from the beginning of the acquisition (24). Axial drift over the course of the acquisition is minimized by engaging the Nikon perfect focus system.

The precision of the localization during a switching cycle is calculated using the Nikon software from the point spread function and the photon count using molecules that are well separated in the sample itself, as well as Alexa 488 and Alexa 647 labeled IgG molecules spread on coverslips, and the values (21 nm for Alexa 488 and 18 nm for Alexa 647) are in agreement with those reported previously (23, 24). A Gaussian fit is used to localize the position of each event to the final super-resolution image. For super-resolution studies on the distributions of sparsely distributed molecules as those presented in this study, the Nyquist resolution is not necessarily relevant, because the molecular structure itself does not allow a high labeling density (25) .

Three-dimensional STORM images were generated by introducing a cylindrical lens in the light path and assigning a Z position based on the shape of the point spread function. The

software also corrects for refractive index mismatch in three-dimensional localization as described (26). To correct for chromatic aberrations due to the objective and the cylindrical lens, the system is pre-calibrated under identical conditions using 4 color Tetraspeck beads. Periodic calibration checks with Tetraspeck beads were performed to ensure quality control and to maintain identical image acquisition conditions for both channels. These corrections are included in the analysis by the Nikon software, as are the corrections for the drift in both XY as well as Z.

Three-dimensional STORM Data Quantification—Images obtained on the Nikon N-storm (Nikon Inc) system were converted to high resolution images, fully calibrated, and imported into Imaris (Bitplane Inc) where they were analyzed using two well established modules: Spots, to mark the centroid location, and Colocalized Spots, to mark and score paired spots that lie within a defined distance from each other in three-dimensional space. Specifically, within the Imaris software we utilized the three-dimensional Spots module to define and mark the centroid of all Rab5 or Rab11 or Munc13-4 fluorescent N-storm positive bright regions of interest (ROI) based on their voxel space. Each ROI from an N-storm system represents a point or cluster of points of a defined intensity and voxel volume, which varies based on both spatial and temporal information acquired at the source. The Colocalized Spots module scored the number of each pair of Rab5 and Munc13-4 and Rab11 and Munc13-4 spots and were binned in the nm distance intervals that we defined.

Neutrophil Stimulation and Flow Cytometry—For flow cytometry studies, 1 million mouse neutrophils were resuspended in phenol red-free RPMI stimulated with human IL8 (250 ng/ml) or left untreated for 1 h at 37 °C. For recovery, the cells were washed with RPMI and resuspended in stimuli-free RPMI for 30 min or 1 h at 37 °C. The reactions were stopped by transferring the samples to ice and immediately spinning down the cells to initiate blocking and staining. To analyze the plasma membrane expression of CXCR2, cells were blocked in ice-cold PBS containing 1% BSA, and stained with PE-conjugated anti-mouse-CxCr2 (R&D Systems) and fluorescein isothiocyanate (FITC)-conjugated anti-Ly6G (clone 1A8, BD Biosciences). The cells were then washed and fixed in 1% paraformaldehyde in PBS. Samples were analyzed using a BD LSR II flow cytometer (BD Biosciences), and the data were processed using FlowJo software.

Superoxide Anion Production—Secretory assays using SLO-permeabilized neutrophils were performed as previously described (21). Briefly, BM-derived mouse neutrophils (1×10^6) were washed twice with phosphate-buffered saline (PBS), resuspended in RPMI, and transferred to a tube containing SLO (2 μl of 2500 units/ml) in the presence of the indicated antibodies (anti-Rab11a cs2413, Cell Signaling; anti-Rab11 610656, BD Transduction Laboratories, or IgG control (5 μg/ml) and incubated at room temperature for 5 min. Where indicated, the cells were incubated with lipopolysaccharide (LPS; 100 ng/ml) for 60 min at 37 °C and stimulated with fMLP (10 μm). Superoxide anion production was continuously monitored using the SOD-inhibitable cytochrome *c* reduction assay at 37 °C as described previously (27).

Antibodies—Primary antibodies used for Western blotting and immunofluorescent staining are: OmicsLink Anti-D tag (Genecopoeia), CGAB-DDK, MPO (Hycult Biotech, Netherlands, HM1051), TLR9 (Thermo, PA5–20203), GFP (Life Technology, A6455), and LAMP1 (sc-19992), Myc (9E10 sc-40), and Munc13-4 (sc-50465) from Santa Cruz Biotechnology. We also utilized anti-Rab11a (Cell Signaling, 2413S), anti-Rab11 (BD Transduction Laboratories, 610656), and anti-Rab5 antibodies (BD Transduction Laboratories 610281).

Statistical Analysis—Data are presented as means, and error bars correspond to standard errors (S.E.) unless otherwise indicated. Statistical significance was determined using the unpaired Student's *t* test or the ANOVA test using GraphPad InStat (version 3) or Excel software, and graphs were made using GraphPad Prism (version 4) software.

Results

Despite its characterization as a Rab27a effector, Munc13-4 regulates important Rab27a-independent functions including the modulation of the secretion of readily releasable secretory vesicles (12), phagosomal maturation (15), and the differential secretory response to stimuli of lytic granules (16). To determine whether Munc13-4 mediates any regulatory function by binding to Rab GTPases other than Rab27a, we developed a screening approach to identify new binding partners of Munc13-4. To this end, we designed a lantha-based time-resolved fluorescence binding assay to identify Munc13-4-interacting Rab GTPases (Fig. 1*A*). The assay is based on the use of non-denaturing lysing mechanisms that conserve the integrity of the intracellular organelles to preserve the natural binding environment so that it measures dynamic interactions in real time. In these assays, Flag-tagged Munc13-4 and EGFP-tagged Rabs are co-expressed in mammalian cells, and lysates are prepared using non-denaturing procedures (Fig. 1*A*). The cells are harvested in a buffer that mimics physiological conditions and lysed by nitrogen cavitation, a method that disrupts the plasma membrane but preserves intracellular organelles and minimizes lysosomal protease release (19). Importantly, the use of cell lysates obtained by nitrogen cavitation favors the analysis of secretory protein interactions in an intact intracellular environment. Thus, Rab proteins remain associated with secretory vesicles and interact with their effectors on the vesicle surface in their natural environment.

Here, we analyzed the binding of Munc13-4 to endocytic Rab GTPases. From all the Rab proteins analyzed, Munc13-4 showed specific binding only to Rab11a and mild interaction with Rab22a but not to other Rab GTPases including Rab5, Rab7, and Rab34, with the exception of Rab27a which served as a positive control. The signal from the binding of Munc13-4 to Rab11a or to the constitutively active mutant Rab11Q70L was significantly higher than that observed for Rab27a even in its constitutive active form (Fig. 1*B*) supporting that Munc13-4 can potentially operate as a Rab11 effector.

To demonstrate that the binding of Rab11 to Munc13-4 is indeed GTP-dependent, we took an independent approach. In these experiments, we utilized recombinant GST-Rab11 (unloaded) or GTPγS-loaded Rab11 (Rab11-GTPγS) to displace the bound (EGFP-) Rab11 from Munc13-4. In Fig. 1*C* we

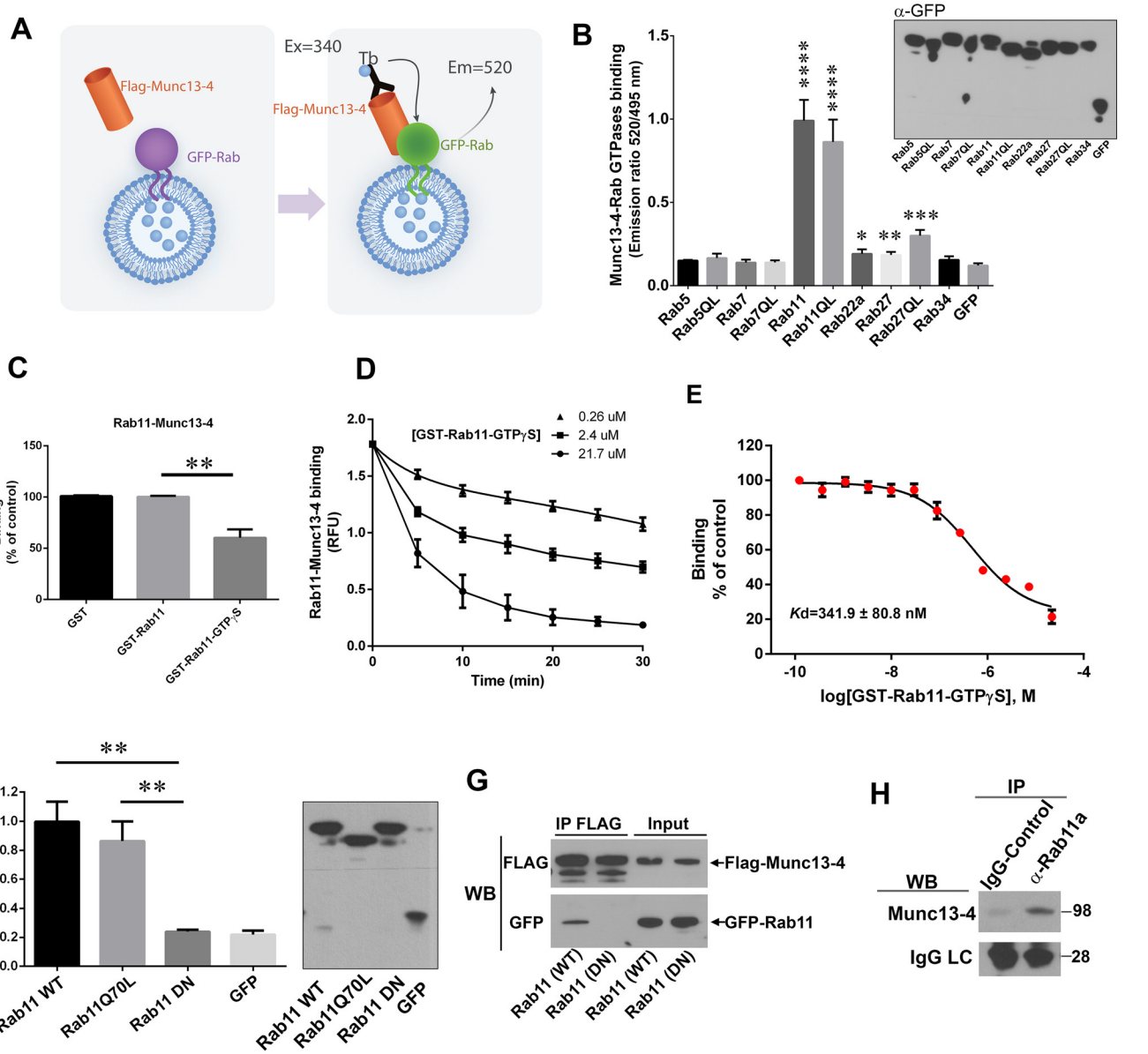

FIGURE 1. **Munc13-4 binds to wild type Rab11 but not to the point-mutant, dominant negative, Rab11S25N.** *A*, schematic representation, TR-FRET assay. Flag-tagged Munc13-4 and EGFP-tagged Rabs are co-expressed in 293T cells, and lysates are prepared under non-denaturing conditions as described under "Experimental Procedures." The reactions are started by addition of the terbium cryptate-conjugated anti-Flag antibody (Cisbio) and carried out at 21 °C. The emission ratio of the acceptor (GFP, 520 nm)/donor (Tb, 495 nm) is indicative of protein binding. *B*, binding of Munc13-4 to the indicated Rab GTPases was analyzed as described in *A*. The results are mean ± S.E. from three to seven experiments performed in triplicates. *, $p = 0.02$; **, $p = 0.01$; ***, $p = 0.0003$; and ****, $p < 0.0001$ *versus* GFP control. *Inset*, GFP-Rab protein expression. *C*, binding of Munc13-4 to wild type Rab11 is competed by GTPγS-loaded recombinant Rab11. In these assays 0.27 nmol of the indicated recombinant proteins were used in 15 μl of TR-FRET reactions. **, $p < 0.01$. *D* and *E*, homologous competitive binding experiments for Rab11 using the TR-FRET assay. Time- (*D*) and dose-response (*E*) competitive binding assays were performed using the indicated concentrations of GTPγS-loaded GST-Rab11. Specific binding of a constant concentration of EGFP-Rab11 in the presence of various concentrations of GST-Rab11 was measured. IC_{50} values were determined using a concentration of EGFP-Rab11 of 79 nM (determined by Western blot), so that the concentration of EGFP-Rab11 was less than half the IC_{50}. K_d was then calculated using the homologous competitive binding curve fitted to a built-in equation of one-site competition (GraphPad Prism). The assay assumes that GST-Rab11 and EGFP-Rab11 have similar affinity for Munc13-4. Error bars correspond to S.E. of three (*D*) or six biological replicates from two independent experiments (*E*). *F*, *left panel*, the binding of Munc13-4 to wild type Rab11 or to the point-mutants constitutively active Rab11Q70L and dominant negative Rab11S25N (DN) was analyzed by TR-FRET as described under "Experimental Procedures." Mean ± S.E. of three independent experiments. **, $p = 0.01$. The level of protein expression in the lysates was analyzed by Western blot (*right panel*). *G*, binding of Munc13-4 to Rab11 or Rab11S25N was analyzed by co-immunoprecipitation assay (IP). The data is representative of two independent experiments with similar results. *WB*, Western blot. *H*, co-immunoprecipitation analysis of endogenous proteins. Human neutrophil lysates (1 mg of total protein) were incubated in the presence of specific anti-Rab11a or IgG control rabbit mAbs as described under "Experimental Procedures," and the pull-downs were analyzed for the presence of Munc13-4 by Western blot (*WB*). Similar amounts of specific and control mAbs were visualized by detection of the antibody light chain (*LC*).

show that while unloaded Rab11 does not compete with recycling endosome-associated EGFP-Rab11, Rab11-GTPγS efficiently competes for Munc13-4 binding. In addition, time course experiments suggest that maximum competition is reached at 30 min of incubation time, further supporting that the binding is dynamic in nature (Fig. 1*D*). Next, using a homologous competitive binding assay, we have estimated a relative K_d for Rab11-Munc13-4 binding under physiological conditions (*i.e.* in lysates containing intact organelles and endogenous competitors) (Fig. 1*E*). The value (K_d = 341.9 ± 80.8 nM)

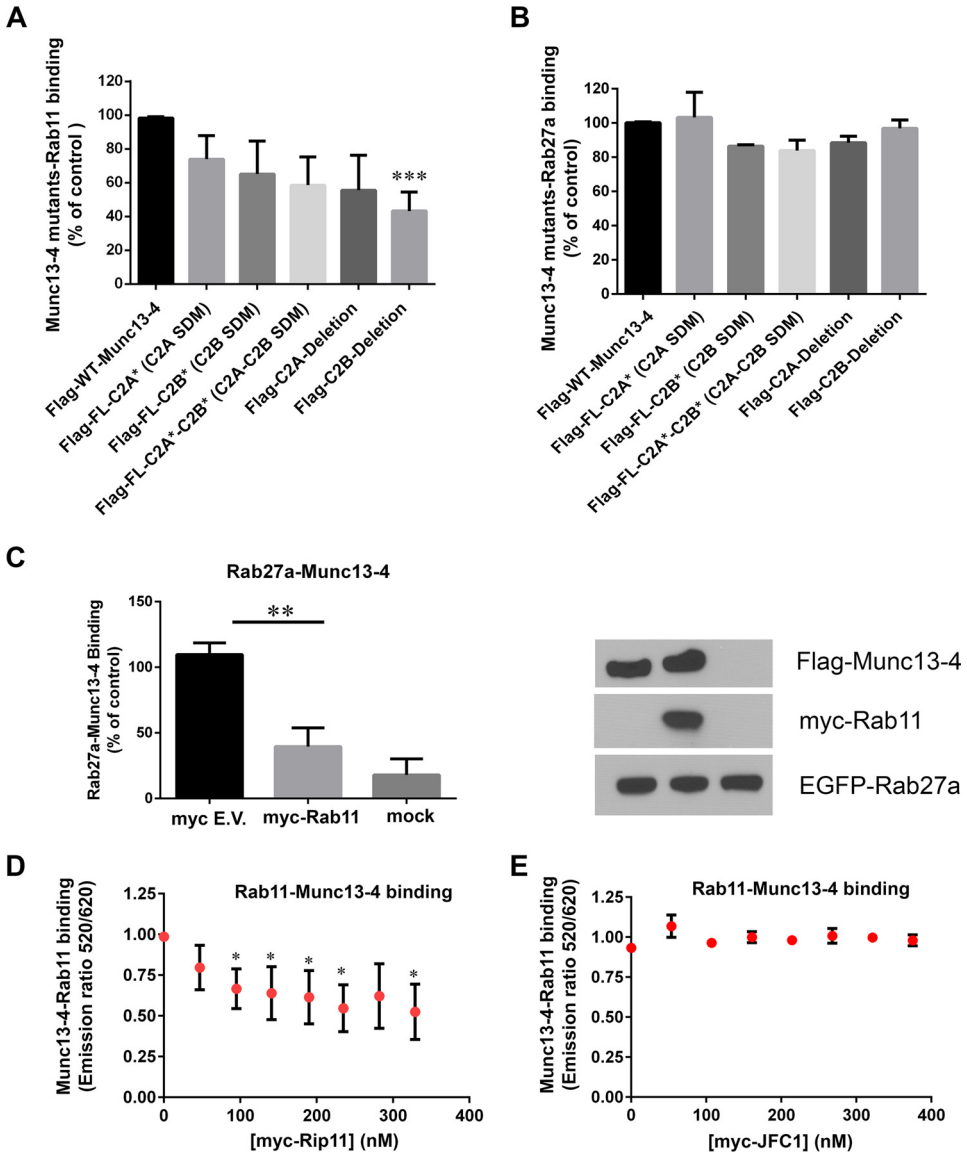

FIGURE 2. **Identification of molecular determinants in Munc13-4 that are important for Rab11 binding.** *A*, the indicated Munc13-4 mutants and truncations were used in the TR-FRET binding assays together with Rab11, and the reactions were carried out as described under "Experimental Procedures." C2A*, includes point mutations Asp-127 and Asp-133 to alanines in the Munc13-4 C2A domain, which knocks out the Ca^{2+}-binding sites in this domain; C2B*, includes point mutations Asp-941 and Asp-947 to alanines to knock out the Ca^{2+}-binding sites in the C2B domain. C2A*C2B* includes 4 Asp → Ala mutations corresponding to both C2 domains. SDM (site-directed mutagenesis). For truncation of the C2A domain (Flag-C2A-deletion) or the C2B domain (Flag-C2B-deletion), amino acids 1–301 or 901–1090 are deleted from Munc13-4, respectively. Equal loading was evaluated by Western blot (data not shown). Data are expressed as mean ± S.E. from three independent experiments. ***, $p = 0.008$. *B*, binding of Munc13-4 mutants and truncations to Rab27a was evaluated by the TR-FRET assay as described in *A*. Data are expressed as mean ± S.E. from three independent experiments. *C*, *left panel*, Rab11 competes with Rab27a for binding to Munc13-4. TR-FRET reactions were performed using lysates from EGFP-Rab27a-expressing cells co-transfected with Flag-Munc13-4 and myc-Rab11 or control empty vectors. **, $p < 0.01$. $n = 3$. *Right panel*, control of protein expression. *D*, competitive binding assays were performed in reactions containing 400 nM Flag-Munc13-4 and increasing concentrations of the Rab11 effector myc-Rip11. Mean ± S.E. from three independent experiments. *, $p < 0.05$. *E*, competitive Rab11-Munc13-4 binding reactions were carried out as described in *D* except that increasing concentration of the Rab27a effector myc-JFC1, used here as a negative myc-tagged control, were included instead of Rip11 in the reactions.

is in the range of K_d values previously described for the binding affinity of Rab11a for MyoVb (254 nM), FIP3 (290 nM), and FIP2 (250 nM) (28–30), respectively.

Finally, Munc13-4 bound to wild type Rab11a (hereon Rab11) but not to the point-mutant, dominant negative Rab11S25N supporting the specificity of the binding reaction (Fig. 1*F*). The binding of Munc13-4 to Rab11 was confirmed using a biochemical approach consisting of the co-immunoprecipitation of these two proteins. In Fig. 1*G*, we show that Munc13-4 is able to pull down wild type Rab11 but not the dominant negative mutant Rab11S25N. In addition, we were able to co-immunoprecipitate the endogenous proteins from neutrophil lysates (Fig. 1*H*). Altogether, our data suggest that Munc13-4 is a Rab11 effector and that Rab11 binding to Munc13-4 requires both association to GTP and accurate subcellular distribution.

Next, to better characterize the Munc13-4 domains involved in Rab11 recognition, we performed experiments using truncated forms of Munc13-4. Truncation of the C2B domain of Munc13-4 (amino acids 901–1090 are deleted from the C ter-

minus, Flag-C2B-deletion) inhibits binding to Rab11 (Fig. 2*A*). However, point mutations at the aspartic acids Asp-127 and Asp-133 to alanines in loop 1 of the Munc13-4 C2A domain (C2A SDM) or in residues Asp-941 and Asp-947, to knock out the Ca^{2+}-binding site in loop 1 of the C2B domain (C2B SDM) or mutations in both (C2A-C2B SDM) had no significant effect on binding (Fig. 2*A*), suggesting that the C2B domain of Munc13-4 is important for binding to Rab11 in a calcium-independent manner. Truncations of the C2A domain or the C2B domain did not inhibit the binding of Munc13-4 to Rab27a (Fig. 2*B*), suggesting that the molecular domains involved in the binding of Munc13-4 to these two GTPases are different.

To determine whether Rab11 competes with Rab27a for Munc13-4 binding, the two GTPases were co-expressed as myc-tagged Rab11 and EGFP-tagged Rab27a and we analyzed the binding of Munc13-4 to Rab27a by TR-FRET. In Fig. 2*C* we show that Rab11 effectively competes with Rab27a for Munc13-4 binding.

Additional competitive assays show that the binding of Munc13-4 to Rab11 is decreased but not abolished by the Rab11 effector Rab11-interacting protein (Rip11/FIP5) (Fig. 2*D*). Contrarily, the Rab27a effector JFC1, used here as a myc-tagged negative control, was ineffective in inhibiting the binding of Munc13-4 to Rab11 at the indicated concentrations (Fig. 2*E*). These data further confirm the specificity of the TR-FRET reaction for the detection of the binding of Rab11 to its effector proteins and suggest that Munc13-4 and Rip11 may compete for Rab11 binding.

Munc13-4 plays a central role in the function of innate immune cells by regulating tethering, docking, and fusion of secretory organelles at the plasma membrane (8, 9, 31). Interestingly, in neutrophils, Munc13-4 regulates the fusion of readily releasable secretory organelles in a Rab27a-independent manner (12), although the molecular mechanism of this regulation is currently unknown. Here, to determine the possible interaction between Rab11 and Munc13-4, we first analyzed the distribution of endogenous Munc13-4 at Rab11-positive compartments in neutrophils. To analyze the subcellular distribution of Rab11 and Munc13-4 in detail, we utilized single-molecule super-resolution microscopy (dSTORM). In Fig. 3*A*, we show that Munc13-4 is distributed in close proximity to Rab11 but not to Rab5, used here as a negative control. Quantitative analysis indicates that ~40% of Munc13-4 molecules are located at distances that are <100 nm from Rab11, a value that is significantly increased compared with Rab5 (Fig. 3*B*). Considering that these assays involve the use of primary and secondary detection antibodies which may increase the apparent distance between endogenous proteins, our high-resolution microscopy assay suggest that Munc13-4 and Rab11 pairs localize at distances that are compatible with, *in situ*, endogenous protein-protein interaction. Importantly, quantification analyses were performed after drift correction. The details of the acquisitions are described under "Experimental Procedures," and an example of drift correction is shown in Fig. 3*C*. Altogether, our data suggest that Munc13-4 associates with Rab11-positive compartments but not with Rab5-positive early endosomes.

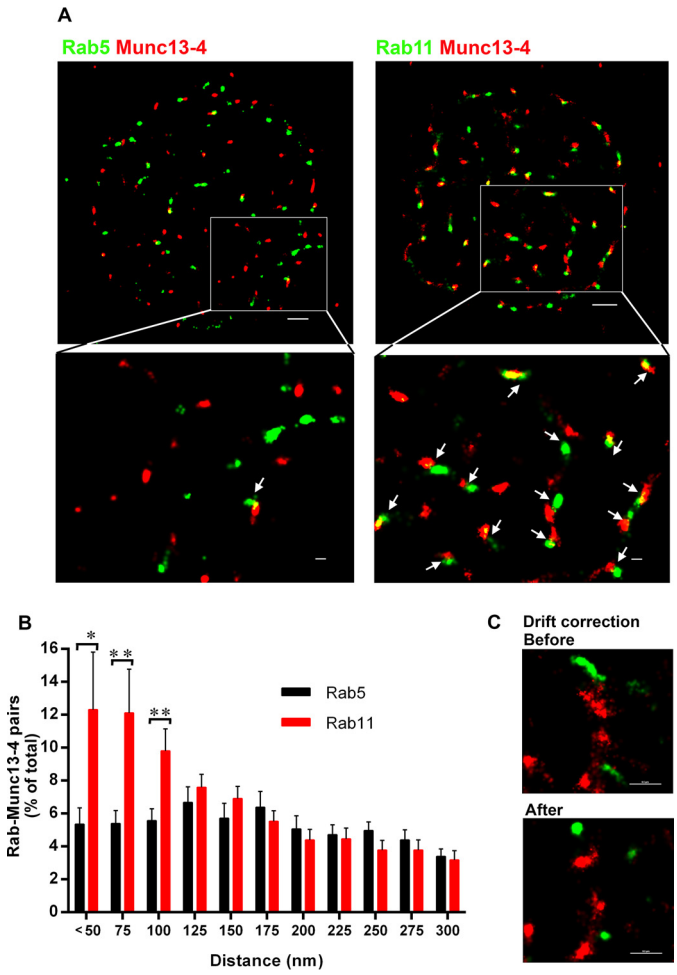

FIGURE 3. **Super-resolution microscopy shows adjacent distribution of endogenous Munc13-4 and Rab11 in primary neutrophils.** *A*, subcellular localization of endogenous Munc13-4 (*red*) and Rab5 (*A*) or Rab11 (*B*) (*green*) was analyzed by direct STORM as described under "Experimental Procedures." Single-molecule Munc13-4 was detected adjacent to Rab11 but rarely to Rab5. Scale bars: whole cell images, 1 μm; magnified images, 200 nm. *B*, quantification of the distance between Rab11 and Munc13-4 centroids was performed as described under "Experimental Procedures," and results were expressed by binning the distance between pairs in 25- nm increments and plotted as a percentage of total pairs at the given distance for each cell. A total of 9121 and 11703 Munc13-4-Rab5 and Rab11 pairs were analyzed, respectively, from 7 independent cells from three independent experiments. Mean ± S.E. *, $p < 0.05$ and **, $p < 0.01$. *C*, example of drift correction. dSTORM images were processed using Nikon software to correct for drift during acquisition as described under "Experimental Procedures."

Next, we utilized immunofluorescence analysis to further elucidate the identity of neutrophil compartments expressing endogenous Rab11. Neutrophils contain five types of secretory organelles including secretory vesicles, azurophilic or primary granules, specific or secondary granules, gelatinase or tertiary granules, and LAMP1-positive late endosomes. Here, we first show that endogenous Munc13-4 colocalizes with Rab11, further linking Munc13-4 with Rab11-regulated mechanisms (Fig. 4*A*). Next, we show that Rab11 has virtually no colocalization with MMP-9, suggesting that Rab11 does not regulate trafficking of secondary or tertiary (gelatinase B-positive) granules (Fig. 4*B*). Poor colocalization was also observed between Rab11 and MPO (12), LAMP1, TNFα, and galectin 3 (data not shown). Contrarily, Rab11 colocalized with a subset of granules expressing $p22^{phox}$, a membrane-associated subunit of the NADPH

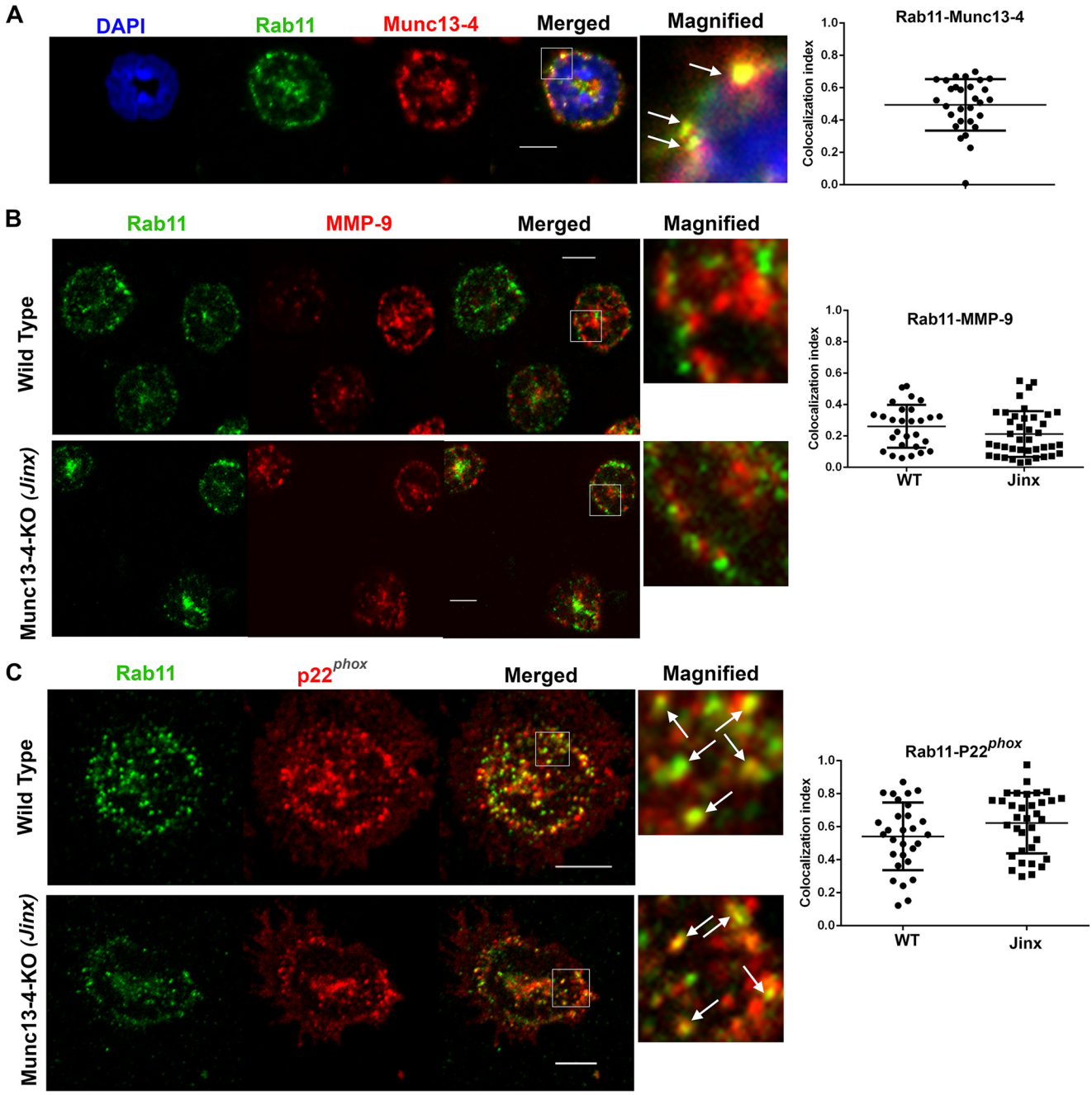

FIGURE 4. **Immunofluorescence analysis of endogenous proteins identify Munc13-4 and p22^{phox} vesicles as Rab11-positive organelles in neutrophils.** *A*, immunofluorescence analysis and quantification of the distribution of endogenous Munc13-4 and Rab11 in mouse primary neutrophils showing that Munc13-4 colocalizes with Rab11. Scale bars: 5 μm. *B*, immunofluorescence analysis and quantification showing lack of colocalization of Rab11 and gelatinase B (MMP-9) in either wild type (*upper panel*) or Munc13-4 KO (*Jinx*) (*lower panel*) cells. *C*, immunofluorescence analysis showing colocalization of Rab11 with a subpopulation of p22^{phox}-positive granules in both wild type (*upper panel*) and Munc13-4-KO (*Jinx*) (*lower panel*) neutrophils. *Arrows* indicate areas of colocalization. *A–C*, quantification of colocalization index was performed using ZEN-LSM software. *A*, 29 cells, two independent experiments; *B*, 28 WT and 40 Jinx cells from three independent experiments and *C*, 30 WT and 34 Jinx, two independent experiments. Mean ± S.D.

oxidase cytochrome b_{558} that neutrophils express in secretory vesicles in addition to secondary granules and tertiary granules (Fig. 4*C*).

Because Rab11 localizes at p22^{phox}-positive vesicles and interacts with Munc13-4, which regulates the oxidase activity by controlling the expression of cytochrome b_{558} at the plasma membrane (15), we evaluated whether Rab11 regulates the activation of the oxidase in primary neutrophils. To this end, we utilized an experimental approach consisting of the permeabilization of neutrophils using the streptococcal exotoxin streptolysin-O (SLO) and interfered with Rab11 function by introducing specific inhibitory anti-Rab11 antibodies. Supporting this approach, previous studies show that the efficiency of the exocytic process in SLO-permeabilized neutrophils is functionally coupled to the formyl-methionyl-leucyl-phenylalanine (fMLP) receptor (32) and that the ultrastructure of neutrophils is largely preserved in SLO-permeabilized neutrophils (11, 33). In addition, SLO-permeabilized neutrophils were utilized pre-

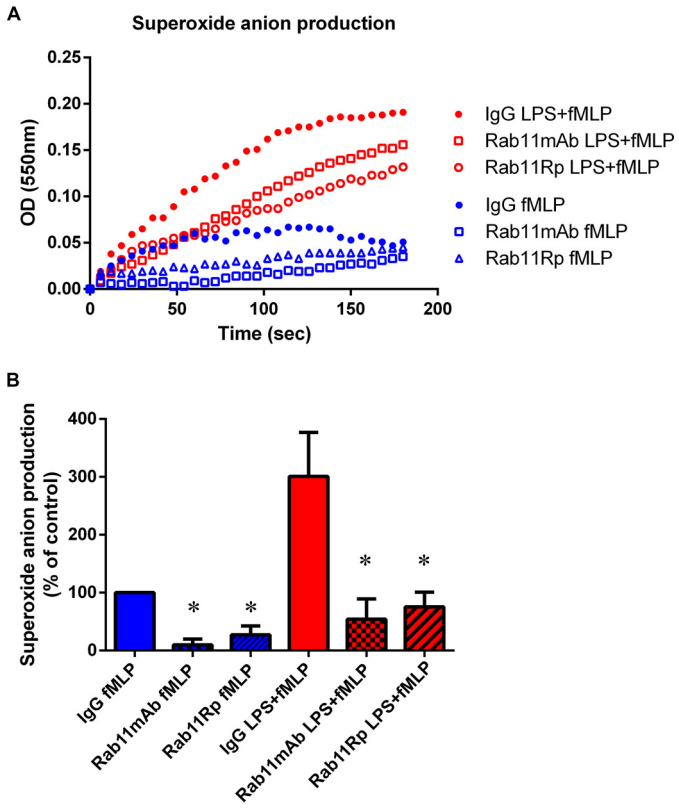

FIGURE 5. **Rab11 regulates the NADPH oxidase activity at the plasma membrane in neutrophils.** Neutrophils were permeabilized using streptolysin O and incubated in the presence of anti-Rab11 (Rab11 mAb and Rab11 rabbit polyclonal, Rp) or control antibodies (IgG). Neutrophils were then washed and stimulated with fMLP either in the absence (*blue symbols*) or the presence of the TLR4 agonist LPS, a priming agent (*red symbols*), and extracellular superoxide anion production was evaluated by the cytochrome *c* reduction assay as described under "Experimental Procedures." *A*, representative kinetics of the reactions are shown. *B*, results are presented as the mean ± S.E. of three independent experiments with similar results. *Rab11mAb*, anti-Rab11 monoclonal antibody; *Rab11Rp*, anti-Rab11 rabbit polyclonal antibody. *IgG*, rabbit IgG control. *B*, superoxide anion production was evaluated as described in *A*. *, $p < 0.05$ *versus* IgG control for the same stimuli.

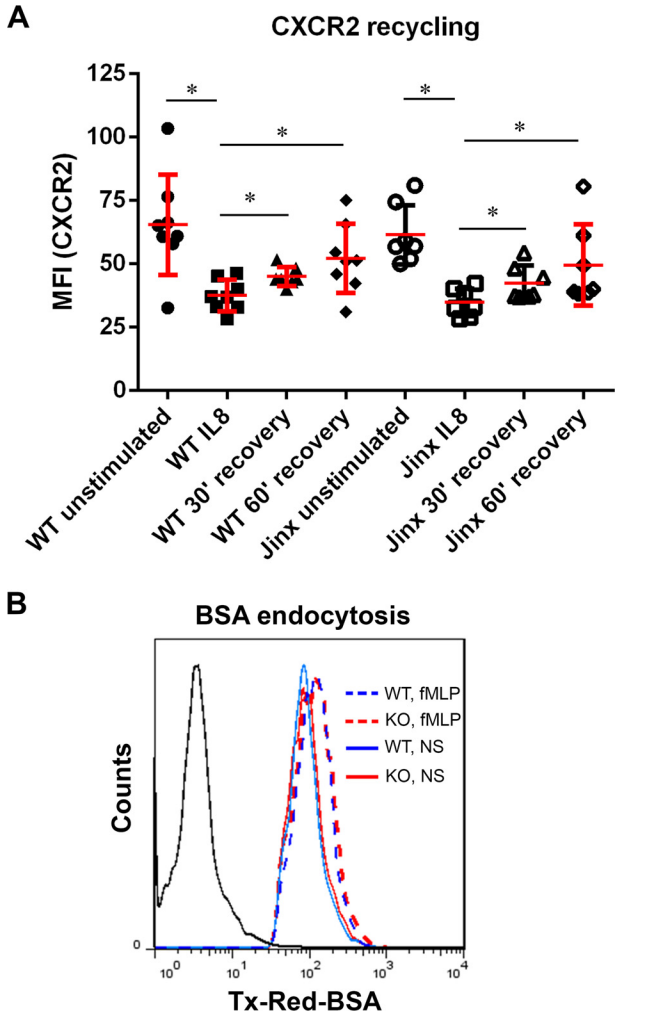

FIGURE 6. **Recycling of CXCR2 receptor is not regulated by Munc13-4 in neutrophils.** *A*, WT or Munc13-4-KO (*Jinx*) neutrophils were incubated in the presence or absence of human IL-8 for 1 h followed by removal of the stimuli and subsequent incubation of the cells in stimuli-free medium for an additional period of 30 (30 recov) or 60 min (60 recov) at 37 °C. The expression of CXCR2 at the plasma membrane was analyzed by flow cytometry as indicated in "Experimental Procedures." $n = 8$ mice per condition were analyzed in four independent experiments. *, $p < 0.05$. b, WT or Munc13-4-KO (*KO*) neutrophils were incubated in the presence of fluorescently labeled BSA and stimulated with fMLP or left untreated (*NS*). Extracellular fluorescent BSA was quenched with trypan blue and the cells were analyzed by flow cytometry. Representative histograms are shown. Unstained control shown to the left (*black line*).

viously to demonstrate the participation of JFC1 and GMIP in azurophilic granule exocytosis in human and murine neutrophils (11, 21). To evaluate the function of Rab11 under physiological conditions, permeabilized neutrophils were incubated with anti-Rab11 inhibitory antibodies and subsequently stimulated with the bacteria-derived mimetic peptide fMLP to induce the activation of the oxidase at the plasma membrane. In Fig. 5, we show that interference with Rab11 function inhibits the extracellular production of superoxide anion in primary neutrophils. The inhibitory effect was further manifested in neutrophils primed with the bacteria-derived TLR4 agonist LPS to amplify the oxidative response when subsequently stimulated with fMLP. These experiments demonstrate for the first time that Rab11 regulates the activity of the oxidase in neutrophils, most likely by controlling the mobilization of a subpopulation of $p22^{phox}$- and Rab11-positive vesicles to the plasma membrane.

Previous studies showed that the recycling of the IL-8 receptor CXCR2 is a mechanism regulated by Rab11 (34). To determine a possible role for Munc13-4 in Rab11-dependent trafficking of recycling compartments, Munc13-4-deficient primary neutrophils were analyzed for their ability to mobilize CXCR2. To this end, wild type or Munc13-4-deficient neutrophils were incubated in the presence or absence of human IL-8 for 1 h followed by removal of the stimuli and subsequent incubation for an additional period of 30 or 60 min at 37 °C. In Fig. 6, we show that both wild type and Munc13-4 KO cells internalized the CXCR2 receptor after 60 min treatment with IL-8, suggesting that CXCR2 endocytosis is a Munc13-4-independent mechanism (Fig. 6*A*, *columns 2* and *6*). The lack of involvement of Munc13-4 in the early stages of endocytosis is in agreement with our data showing lack of colocalization between Munc13-4 and Rab5, the small GTPase that regulates early endosome trafficking (Fig. 3) or with its effector EEA1 (12). This was also confirmed by our data from an independent approach showing that Munc13-4-KO neutrophils endocytose BSA as

efficiently as wild type neutrophils either under stimulated or unstimulated conditions (Fig. 6*B*). Next, to evaluate the recycling of CXCR2, we removed the ligand from the reaction medium and determined the up-regulation of the receptor at the plasma membrane by flow cytometry. Thirty minutes after the removal of IL-8 from the incubation medium, we observed CXCR2 recycling at the plasma membrane, a process that was further emphasized after 60 min-recovery time (Fig. 6*A*). No differences in CXCR2 recycling at the plasma membrane were observed between wild type and Munc13-4 knock-out cells, indicating that CXCR2 recycling is a Munc13-4-independent mechanism.

To better understand the mechanisms mediated by Munc13-4 in the regulation of Rab11-positive vesicle trafficking, we utilized live cells to analyze the subcellular localization of Rab11 and Munc13-4 in a spatiotemporal manner by total internal reflection fluorescence microscopy (TIRFM) (35). Here, we show that Munc13-4 colocalizes with Rab11-positive vesicles in retinal pigment epithelial cells (Fig. 7*A* and supplemental movie S1). Noteworthy, the Munc13-4 double mutant, Munc13-4-C2A*B*, a dominant negative for calcium binding, also colocalized with Rab11 (Fig. 7*B* and supplemental movie S2), a result that is in agreement with our data showing that these mutations in the C2 domains did not significantly affect Munc13-4-Rab11 binding (Fig. 2*A*). Quantitative analysis of vesicular dynamics shows that Munc13-4 regulates Rab11 trafficking as Rab11-contatining vesicles have enhanced motility in cells expressing Munc13-4-C2A*B* (Fig. 7*C*). Thus, the expression of this Munc13-4 mutant with defective calcium-binding domains induces faster movement of Rab11-positive vesicles in the plane parallel to the plasma membrane. Because Munc13-4 binding to SNARE proteins depends on the mutated residues (8), the increment in Rab11 vesicle speed induced by the calcium binding-deficient mutant of Munc13-4 is most likely caused by interfering with the function of Munc13-4 as a tethering effector. These data suggest that Rab11-positive vesicles may utilize Munc13-4 in the final step of exocytosis, *i.e.* by mediating tethering or docking at the plasma membrane.

To analyze whether endogenous Munc13-4 regulates the vesicular dynamics of Rab11-positive organelles in primary neutrophils, we transfected wild type or Munc13-4-KO neutrophils with the expression vector EGFP-Rab11 and analyzed vesicular trafficking by TIRFM. First, we show that Rab11 localizes at small, fast moving vesicles in transfected neutrophils (Fig. 8). Importantly, no significant morphological differences of Rab11-positive compartments were observed in neutrophils lacking Munc13-4 expression as compared with wild type neutrophils, neither in static (Fig. 8*A*) nor dynamic (supplemental movies S3 and S4) imaging analyses. However, a larger number of slow moving Rab11-positive vesicles were detected in close proximity to the PM in wild type cells as compared with Munc13-4-KO neutrophils (Fig. 8*A*, *arrows*). Quantitative vesicular dynamic analysis demonstrate that in the absence of Munc13-4, Rab11-positive vesicles move at a higher speed (Fig. 8*B*). In addition, we observed a significantly decreased number of Rab11-positive vesicles with motility restriction (speed under 0.15 μm/s) in Munc13-4-KO neutrophils. Contrarily, no significant differences were observed in Rab11-positive vesicle dynamics in neutrophils lacking Rab27a expression (*ashen*) (Fig. 8*C*) further suggesting that Rab27a does not affect Rab11 trafficking. All together, these results further support a possible role for Munc13-4 in the docking of Rab11-positive vesicles in neutrophils.

Rab11 directly regulates exocytosis of non-endocytic, secretory compartments (36–38). To formally demonstrate a possible role for Munc13-4 in Rab11-positive vesicle docking in neutrophils, we studied the regulation of Rab11-expressing vesicles at the plasma membrane using TIRFM. In these experiments, we quantitatively analyzed the distribution of Rab11 at the exocytic active zone in wild type and Munc13-4-KO neutrophils. To study the neutrophil exocytic function, we activated the protein kinase C signaling pathway to induce a phosphorylation cascade, a mechanism known to induce neutrophil exocytosis (12) and to mediate exocytosis and transcytosis of Rab11 vesicles (17, 39). Here, we show that PMA-stimulated Munc13-4 KO cells display a significantly reduced number of Rab11-positive secretory vesicles at the plasma membrane when compared with stimulated wild type cells (Fig. 9, *A* and *B*), further suggesting that the mobilization of Rab11-positive vesicles at the exocytic active zone in close proximity to the plasma membrane and the docking of Rab11-positive vesicles at the PM are Munc13-4-dependent mechanisms. Importantly, despite the fact that Munc13-4 regulates trafficking of Rab27a-positive organelles in neutrophils, the defects in Rab11-positive vesicle trafficking observed here cannot be explained by a putative impairment in Rab27a function, because Rab27a and Rab11 localize entirely at different intracellular compartments in neutrophils, even under stimulated conditions (Fig. 9*C*).

Discussion

In this study, we utilize biochemical assays, cell-based approaches, super-resolution microscopy and functional studies to demonstrate that Munc13-4 is a novel partner of Rab11. Using a newly designed Rab-GTPase-effector binding assay, we demonstrate that Munc13-4 binds to wild type Rab11 but not to a point-mutant dominant negative form of the Rab GTPase. After confirming these results using traditional immunoprecipitation assays, we show that Rab11 and Munc13-4 colocalize at dynamic vesicles in live cells and at the endogenous level in neutrophils. Functional assays demonstrate that Munc13-4 regulates the up-regulation and docking of Rab11-positive vesicles during exocytosis. Altogether, we demonstrate that Munc13-4 regulates cellular functions through a newly identified Rab11-dependent interaction and that Rab11 plays an important role in the regulation of the NADPH oxidase, a central neutrophil innate immune defense mechanism.

Based on the observation that Munc13-4 regulates lytic granule exocytosis and that Munc13-4 deficiency leads to a hemophagocytic syndrome in humans similar to that caused by Rab27a-deficiency, Munc13-4 was originally identified as a Rab27a effector (14). The functional interaction between Munc13-4 and Rab27a was later confirmed in several hematopoietic cells including neutrophils, platelets and mast cells (11, 13, 40, 41). However, in addition to its Rab27a-dependent functions, Rab27a-independent functions were also identified for Munc13-4. For instance, the up-regulation of a subpopulation

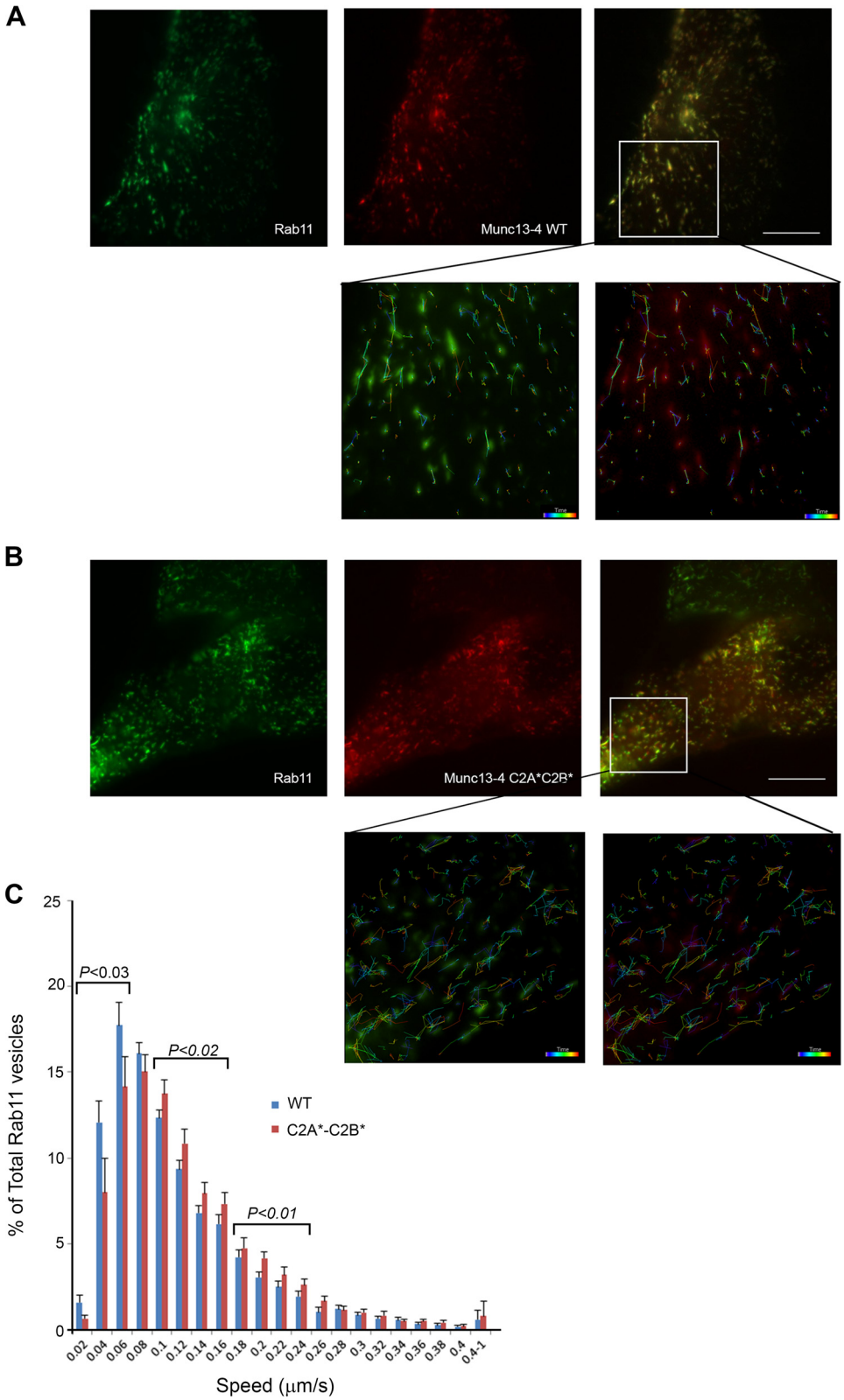

FIGURE 7. **Munc13-4 colocalizes with Rab11 in a spatio-temporal manner and regulates vesicular trafficking of Rab11-positive vesicles.** *A*, live-cell microscopy analysis of the dynamics of Rab11- and Munc13-4-positive vesicles. Representative images of the subcellular distribution of mCherry-Munc13-4 and EGFP-Rab11 evaluated by TIRF microscopy in RPE cells. *B*, live-cell microscopy analysis of the dynamics of Rab11-positive vesicles and the Munc13-4 mutant Munc13-4-C2A*B* (described in Fig. 2). *A* and *B*, *lower panels* show examples of the tracking analysis performed for both channels, confirming identical spatio-temporal distribution of Rab11 and either Munc13-4 or Munc13-4-C2A*B*. *C*, histograms representing the speeds of Rab11-containing organelles in cells expressing either wild type Munc13-4 (*blue bars*) or the mutant Munc13-4-C2A*B* (*red bars*). The speeds for the independent vesicles were binned in 0.02-μm/s increments and plotted as a percentage of total vesicles for a given cell. Results are represented as mean ± S.E. from 18 cells expressing wild type Munc13-4 and 19 cells expressing the Munc13-4-C2A*B* mutant. The statistically significant differences between the two groups are indicated in the figure.

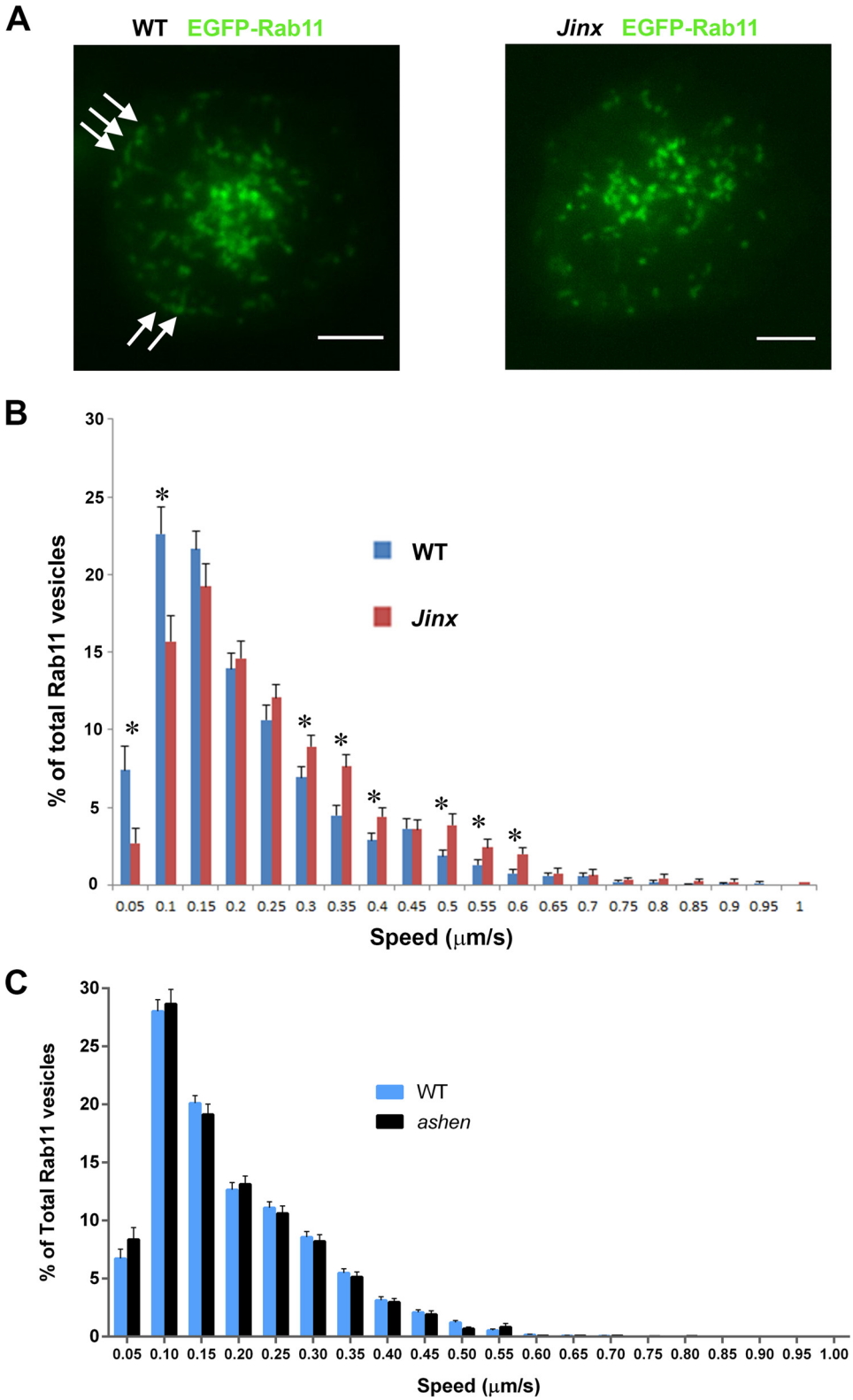

FIGURE 8. **Munc13-4 regulates Rab11-positive vesicular dynamics and tethering in primary neutrophils.** Neutrophils from WT or Munc13-4 KO (Jinx) mice were transfected for the expression of EGFP-Rab11 and vesicular dynamics was analyzed by TIRFM. *A*, representative images of the subcellular distribution of Rab11 in WT and KO cells. The *arrows* indicate Rab11-positive vesicles that appear associated with the plasma membrane in vesicular dynamic studies (see associated supplemental movies S3 and S4). *B*, quantitative analysis of Rab11 dynamics. Histograms representing the speeds of Rab11-containing organelles in wild type (*blue bars*) or Munc13-4 KO neutrophils (*red bars*) are shown. The speeds for the independent vesicles were binned in 0.05-μm/s increments and plotted as a percentage of total vesicles for a given cell. Results are represented as mean ± S.E. from 85 wild type and 93 Munc13-4-KO cells. *, $p < 0.05$. *C*, neutrophils from WT or Rab27a KO (*ashen*) mice were transfected for the expression of EGFP-Rab11, and vesicular dynamics was analyzed by TIRFM. Results from the analysis of 101 wild type and 131 Rab27a KO (*ashen*) cells are depicted. No significant differences in Rab11 vesicular dynamics was observed between wild type and Rab27a KO neutrophils.

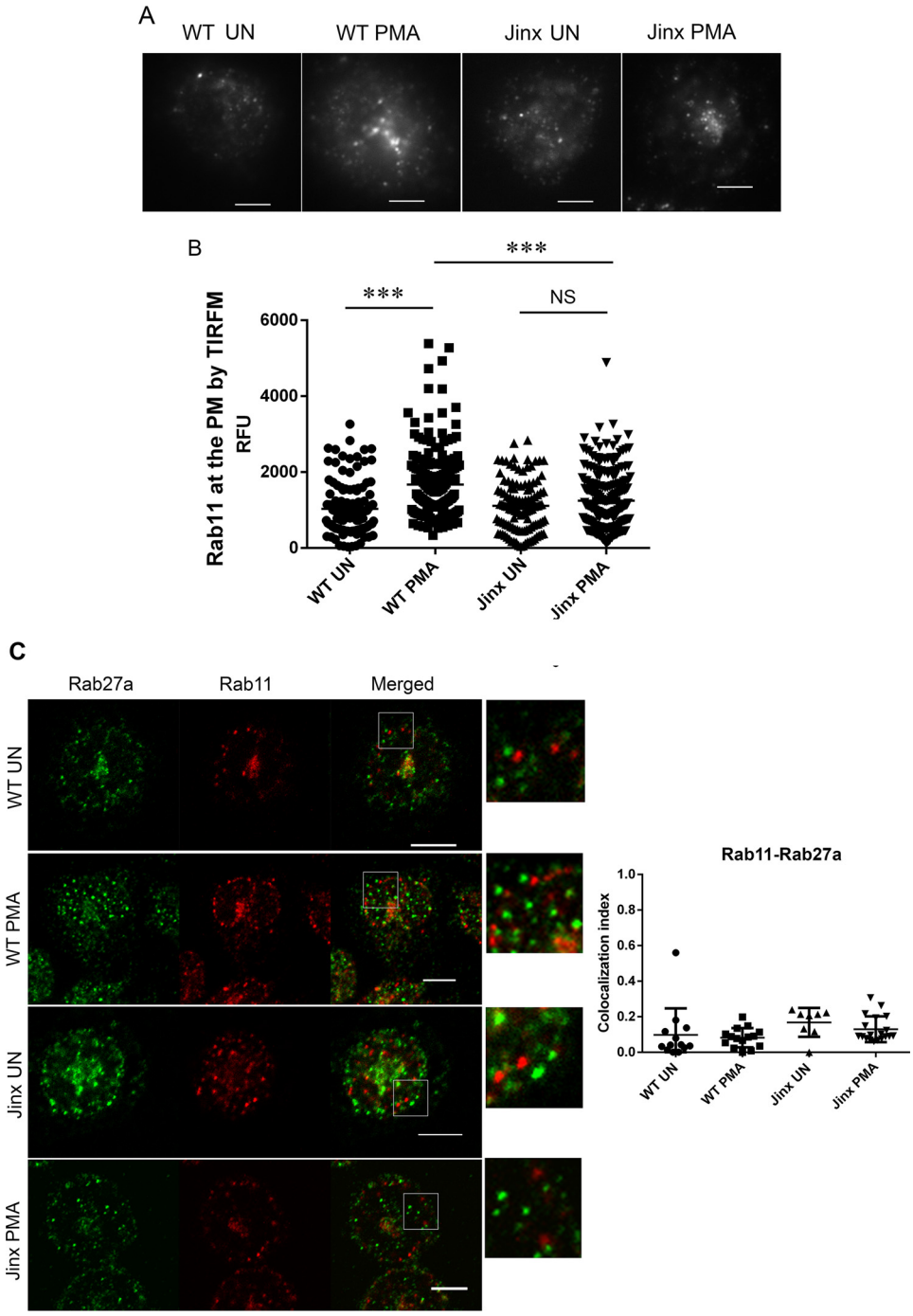

FIGURE 9. **Mobilization of Rab11-positive organelles and docking/retention at the plasma membrane in response to PKC activation is impaired in the absence of Munc13-4 expression.** Neutrophils were stimulated with the PKC agonist PMA, the cells were fixed and stained for the detection of endogenous Rab11 and the distribution of Rab11-positive vesicles at the PM (exocytic active zone, ~100 nm) was analyzed by TIRFM. *A*, representative images of the distribution of endogenous Rab11-positive vesicles in PMA-stimulated or unstimulated WT or Munc13-4-KO (*Jinx*) cells. *B*, quantitative analysis of the distribution of Rab11-positive vesicles. A total of 118, 191, 115, and 219 cells were analyzed for the conditions WT, unstimulated (UN); WT, PMA; Jinx, unstimulated and Jinx, PMA, respectively, in four independent experiments. ***, $p < 0.0001$. *NS*, not significant. *C*, Rab11 and Rab27a localize at independent subcellular compartments in neutrophils. Wild type or KO neutrophils were left untreated or stimulated with PMA as described above, fixed, and stained for endogenous Rab11 and Rab27a using specific antibodies. The magnified images show that Rab11 and Rab27a localize at different compartments in both stimulated and untreated, wild type, and Munc13-4 KO cells. Quantitative analysis of 28 wild type and 27 Munc13-4 KO (*Jinx*) cells was performed using the ZEN-LSM software. Three independent experiments are shown.

of readily-releasable granules at the plasma membrane in response to the TLR4 agonist LPS has been demonstrated in neutrophils (12). Similarly, a Rab27a-independent, stimuli-dependent regulation of lytic granules has also been demonstrated for Munc13-4 in NK cells (16). Interestingly, in another study, Munc13-4 deficiency was shown to induce a defect in lytic granule maturation in CTLs, a process that requires the fusion of Rab11 and Rab27 containing vesicles (10); however, in that study the authors were unable to demonstrate direct interaction between Rab11 and Munc13-4, and the presence of

Munc13-4 at recycling endosomes was suggested to be related to a coordinated endocytic activity (10). Here, we demonstrate for the first time that in addition to its well-known binding to Rab27a, Munc13-4 directly binds to Rab11. We also show that endogenous Munc13-4 and Rab11 are distributed adjacent to each other, as detected by single-molecule, super-resolution microscopy, an observation that is compatible with our suggestion that these molecules directly interact at endogenous levels. In addition, we have functionally linked Munc13-4 to Rab11 as our results also demonstrate that Munc13-4 regulates the trafficking of Rab11-positive organelles and mediates their engagement in exocytosis by inducing tethering or docking at the exocytic active zone. Altogether, our studies not only elucidate the mechanisms regulating Rab11 by Munc13-4 at the molecular level in neutrophils but also contribute insights that may help improve our understanding of the molecular processes regulating exocytosis in other hematopoietic cells. In addition they expand the mechanistic understanding of Munc13-4 function by establishing Munc13-4 as a direct Rab11 effector. Finally, from the data presented here, it becomes clear that a given Rab GTPase or effector may play distinct roles in different hematopoietic cells. Supporting this view, different to that observed in CTLs, Rab11 and Rab27a vesicles do not undergo a process of co-maturation in neutrophils as these GTPases remain distributed at independent compartments through all steps of exocytosis. Similarly, the lysosomal-related organelles of neutrophils (azurophilic granules) do not acquire Rab11 during priming of exocytosis (12). Altogether, our data highlight a functional promiscuity of Munc13-4 as a Rab effector, help explain why some Munc13-4-dependent functions are Rab27a-independent and emphasize the different molecular mechanisms used by similar mediators in diverse hematopoietic cells.

In this study, we use a novel TR-FRET assay to determine the binding of Rab-GTPases to their effectors. Our studies emphasize the importance of using binding approaches that utilize less stringent, non-detergent conditions in the evaluation of molecular interactions involving small Rab GTPases. Thus, in this assay, the binding of the small GTPase to its effector is evaluated in the natural environment, *i.e.* the cytosolic side of the intracellular compartment where the GTPase is docked through its geranyl-geranyl group. In addition, the absence of detergents in the reaction media favors the detection of biologically significant interactions. Finally, the use of TR-FRET allows for the detection of binding events in the intact biological setting and is therefore a better approach to identify meaningful interactions under conditions that are crucial for the execution of the biological function in living cells.

Although not generally considered a "secretory" Rab GTPase, Rab11 has been shown to regulate exocytosis in several biological systems. In bladder umbrella cells, the exocytosis of discoidal/fusiform-shaped vesicles is regulated by a mechanism that involves the recruitment of Rab8 by Rab11 and the participation of the Rab11-interacting protein Myo5B (42). Similarly, Rab11 regulates the secretory process necessary for apical membrane amplification in *Drosophila* photoreceptors. In this mechanism, Rab11, again, was demonstrated to interact with the motor protein Myo5 and with the effector dRip11, the only *Drosophila* class I Rab-FIP. In this system, the Rab11 effector (dRip11) was proposed to regulate a calcium-independent mechanism of Myo5 activation to facilitate cargo transport (37). This differs from the function this small GTPase is proposed to exert in neuronal cells where Rab11 regulates calcium-dependent exocytosis, although it also regulates calcium-independent mechanisms (43). Finally, Rab11 and its effector Rip11 were demonstrated to regulate cAMP-potentiated insulin secretion in pancreatic beta cell lines, a process regulated by PKA-mediated Rip11 phosphorylation (38). Thus, many independent works described a role for Rab11 in regulated exocytosis, and although some of the co-factors and effectors have been identified, the mechanisms regulating the discrete exocytic steps including trafficking and docking of Rab11 vesicle at the PM have remained obscure. Our data suggest that Munc13-4 controls Rab11-positive vesicle trafficking. In particular, we observed that a calcium binding-deficient mutant of Munc13-4 increases the speed of these vesicles in the plane parallel to the plasma membrane. Since the mutated residues are not necessary for Rab11 binding, our data suggest that Munc13-4 mediates the interaction of Rab11-positive vesicles with counter receptors at the plasma membrane thus regulating tethering or docking of Rab11-vesicles and reducing their trafficking speed. A role for Munc13-4 in tethering or docking is further supported by our data showing that the number of Rab11-positive vesicles is up-regulated at the plasma membrane during stimulated exocytosis decreases in cells lacking Munc13-4 expression. Finally, our data showing that Munc13-4 and Rip11 compete for Rab11 binding, together with the data mentioned above that Rip11 regulates exocytosis through mechanisms that involve the motor protein Myo5, may suggest that Rip11 and Munc13-4 would be able to regulate common secretory pathways through sequential binding to Rab11 by controlling actin-mediated trafficking and plasma membrane docking, respectively.

Rab11 plays a fundamental role in the regulation of vesicular trafficking processes associated with the innate immune response. In particular, Rab11 has been proposed to regulate ligand-initiated signaling through the control of receptor recycling (34), the activation of distant regulatory pathways via the secretion of exosomes (44) and the control of inflammatory responses through the regulation of endosomal receptor trafficking and sorting (45). Our data support the view that Rab11 is important for the correct function of immune cells and, in particular, suggest that Rab11 regulates neutrophil exocytosis and ROS production, two essential neutrophil innate immune responses. Our data also suggest that Rab11 regulates neutrophil function through the mobilization of a selective group of Rab11-positive secretory organelles. In this way, we demonstrate that two small GTPases with secretory function, Rab11 and Rab27a, localize at discrete and different subcellular compartments. Since both GTPases bind to and are regulated by Munc13-4, and both, together with Munc13-4, regulate the oxidase activity, our results suggest that neutrophils have evolved to develop alternative yet complementary mechanisms to elicit a function that is at the foremost importance in the mechanism of innate immunity regulation. In neutrophils, secretory organelles are frequently categorized according to their cargo content in addition to the organelle's characteristics of responsive-

ness to secretory stimuli. Our data showing that diverse secretory compartments are enriched in discrete secretory small GTPases with complementary functions highlight the diversity of the populations of secretory organelles in neutrophils and emphasize the need for an additional level of characterization for these organelles based on the granule's trafficking machinery.

In conclusion, we demonstrate that Rab11-vesicle trafficking is regulated by Munc13-4, which emerges as a novel Rab11 effector. We also show that Rab11 localizes at a discrete subpopulation of secretory vesicles associated with important neutrophil functions. Since neutrophil secretory proteins are highly toxic and pro-inflammatory, our data highlight the interaction of Rab11 with Munc13-4 as a potential target for the control of inflammation.

Author Contributions—J. L. J. performed experiments, analyzed data, contributed ideas and, comments and helped write the manuscript; J. H., performed experiments and analyzed data. M. R., contributed ideas and comments and performed experiments. K. J. performed experiments and analyzed data; W. K. analyzed data and performed statistical analyses. J. Z. contributed ideas and comments; S. D. C. designed experiments, performed experiments, analyzed data, and wrote the manuscript with input from J. L. J.

Acknowledgments—We thank Dr. Bruce Beutler for contributing the Munc13-4-KO mouse model. We thank Beverley Ellis for editing, corrections, and comments and Steve Brown for contributing ideas and comments.

References

1. Pfeffer, S. R. (2001) Rab GTPases: specifying and deciphering organelle identity and function. *Trends Cell Biol.* **11,** 487–491
2. Kelly, E. E., Horgan, C. P., and McCaffrey, M. W. (2012) Rab11 proteins in health and disease. *Biochem. Soc. Trans.* **40,** 1360–1367
3. Takahashi, S., Kubo, K., Waguri, S., Yabashi, A., Shin, H. W., Katoh, Y., and Nakayama, K. (2012) Rab11 regulates exocytosis of recycling vesicles at the plasma membrane. *J. Cell Sci.* **125,** 4049–4057
4. Cox, D., Lee, D. J., Dale, B. M., Calafat, J., and Greenberg, S. (2000) A Rab11-containing rapidly recycling compartment in macrophages that promotes phagocytosis. *Proc. Natl. Acad. Sci. U.S.A.* **97,** 680–685
5. Ramel, D., Wang, X., Laflamme, C., Montell, D. J., and Emery, G. (2013) Rab11 regulates cell-cell communication during collective cell movements. *Nat. Cell Biol.* **15,** 317–324
6. Horgan, C. P., and McCaffrey, M. W. (2009) The dynamic Rab11-FIPs. *Biochem. Soc. Trans.* **37,** 1032–1036
7. Koch, H., Hofmann, K., and Brose, N. (2000) Definition of Munc13-homology-domains and characterization of a novel ubiquitously expressed Munc13 isoform. *Biochem. J.* **349,** 247–253
8. Boswell, K. L., James, D. J., Esquibel, J. M., Bruinsma, S., Shirakawa, R., Horiuchi, H., and Martin, T. F. (2012) Munc13-4 reconstitutes calcium-dependent SNARE-mediated membrane fusion. *J. Cell Biol.* **197,** 301–312
9. Feldmann, J., Callebaut, I., Raposo, G., Certain, S., Bacq, D., Dumont, C., Lambert, N., Ouachée-Chardin, M., Chedeville, G., Tamary, H., Minard-Colin, V., Vilmer, E., Blanche, S., Le, Deist, F., Fischer, A., and de Saint Basile, G. (2003) Munc13-4 is essential for cytolytic granules fusion and is mutated in a form of familial hemophagocytic lymphohistiocytosis (FHL3). *Cell* **115,** 461–473
10. Meéager, M. M., Ménasché, G., Romao, M., Knapnougel, P., Ho, C. H., Garfa, M., Raposo, G., Feldmann, J., Fischer, A., and de Saint Basile, G. (2007) Secretory cytotoxic granule maturation and exocytosis require the effector protein hMunc13-4. *Nat. Immunol.* **8,** 257–267
11. Brzezinska, A. A., Johnson, J. L., Munafo, D. B., Crozat, K., Beutler, B., Kiosses, W. B., Ellis, B. A., and Catz, S. D. (2008) The Rab27a Effectors JFC1/Slp1 and Munc13-4 Regulate Exocytosis of Neutrophil Granules. *Traffic* **9,** 2151–2164
12. Johnson, J. L., Hong, H., Monfregola, J., Kiosses, W. B., and Catz, S. D. (2011) MUNC13-4 restricts motility of RAB27A-expressing vesicles to facilitate lipopolysaccharide-induced priming of exocytosis in neutrophils. *J. Biol. Chem.* **286,** 5647–5656
13. Shirakawa, R., Higashi, T., Tabuchi, A., Yoshioka, A., Nishioka, H., Fukuda, M., Kita, T., and Horiuchi, H. (2004) Munc13-4 is a GTP-Rab27-binding protein regulating dense core granule secretion in platelets. *J. Biol. Chem.* **279,** 10730–10737
14. Neeft, M., Wieffer, M., de Jong, A. S., Negroiu, G., Metz, C. H., van Loon, A., Griffith, J., Krijgsveld, J., Wulffraat, N., Koch, H., Heck, A. J., Brose, N., Kleijmeer, M., and van der Sluijs, P. (2005) Munc13-4 is an effector of rab27a and controls secretion of lysosomes in hematopoietic cells. *Mol. Biol. Cell* **16,** 731–741
15. Monfregola, J., Johnson, J. L., Meijler, M. M., Napolitano, G., and Catz, S. D. (2012) MUNC13-4 protein regulates the oxidative response and is essential for phagosomal maturation and bacterial killing in neutrophils. *J. Biol. Chem.* **287,** 44603–44618
16. Wood, S. M., Meeths, M., Chiang, S. C., Bechensteen, A. G., Boelens, J. J., Heilmann, C., Horiuchi, H., Rosthøj, S., Rutynowska, O., Winiarski, J., Stow, J. L., Nordenskjöld, M., Henter, J. I., Ljunggren, H. G., and Bryceson, Y. T. (2009) Different NK cell-activating receptors preferentially recruit Rab27a or Munc13-4 to perforin-containing granules for cytotoxicity. *Blood* **114,** 4117–4127
17. Lindsay, A. J., and McCaffrey, M. W. (2004) The C2 domains of the class I Rab11 family of interacting proteins target recycling vesicles to the plasma membrane. *J. Cell Sci.* **117,** 4365–4375
18. Crozat, K., Hoebe, K., Ugolini, S., Hong, N. A., Janssen, E., Rutschmann, S., Mudd, S., Sovath, S., Vivier, E., and Beutler, B. (2007) Jinx, an MCMV susceptibility phenotype caused by disruption of Unc13d: a mouse model of type 3 familial hemophagocytic lymphohistiocytosis. *J. Exp. Med.* **204,** 853–863
19. Klempner, M. S., Mikkelsen, R. B., Corfman, D. H., and André-Schwartz, J. (1980) Neutrophil plasma membranes. I. High-yield purification of human neutrophil plasma membrane vesicles by nitrogen cavitation and differential centrifugation. *J. Cell Biol.* **86,** 21–28
20. Johnson, J. L., Pacquelet, S., Lane, W. S., Eam, B., and Catz, S. D. (2005) Akt regulates the subcellular localization of the Rab27a-binding protein JFC1 by phosphorylation. *Traffic* **6,** 667–681
21. Johnson, J. L., Monfregola, J., Napolitano, G., Kiosses, W. B., and Catz, S. D. (2012) Vesicular trafficking through cortical actin during exocytosis is regulated by the Rab27a effector JFC1/Slp1 and the RhoA-GTPase-activating protein Gem-interacting protein. *Mol. Biol. Cell* **23,** 1902–1916
22. Napolitano, G., Johnson, J. L., He, J., Rocca, C. J., Monfregola, J., Pestonjamasp, K., Cherqui, S., and Catz, S. D. (2015) Impairment of chaperone-mediated autophagy leads to selective lysosomal degradation defects in the lysosomal storage disease cystinosis. *EMBO Mol. Med.* **7,** 158–174
23. Rust, M. J., Bates, M., and Zhuang, X. (2006) Sub-diffraction-limit imaging by stochastic optical reconstruction microscopy (STORM). *Nature Methods* **3,** 793–795
24. Huang, B., Wang, W., Bates, M., and Zhuang, X. (2008) Three-dimensional super-resolution imaging by stochastic optical reconstruction microscopy. *Science* **319,** 810–813
25. Xu, K. S., Sang-Hee; Zhuang, Xiaowei (2013) Super-Resolution Imaging Through Stochastic Switching and Localization of Single Molecules: An overview. in *Far-field Optical Nanoscopy* (Tinnefeld, P., Eggeling, C., and Hell, S. W., eds), pp. 27–64, Springer Berlin Heidelberg
26. Huang, B., Jones, S. A., Brandenburg, B., and Zhuang, X. (2008) Whole-cell 3D STORM reveals interactions between cellular structures with nanometer-scale resolution. *Nature Methods* **5,** 1047–1052
27. Markert, M., Andrews, P. C., and Babior, B. M. (1984) Measurement of O2- production by human neutrophils. The preparation and assay of NADPH oxidase-containing particles from human neutrophils. *Methods Enzymol.* 358–365
28. Pylypenko, O., Attanda, W., Gauquelin, C., Lahmani, M., Coulibaly, D., Baron, B., Hoos, S., Titus, M. A., England, P., and Houdusse, A. M. (2013)

Structural basis of myosin V Rab GTPase-dependent cargo recognition. *Proc. Natl. Acad. Sci. U.S.A.* **110,** 20443–20448
29. Eathiraj, S., Mishra, A., Prekeris, R., and Lambright, D. G. (2006) Structural basis for Rab11-mediated recruitment of FIP3 to recycling endosomes. *J. Mol. Biol.* **364,** 121–135
30. Lall, P., Horgan, C. P., Oda, S., Franklin, E., Sultana, A., Hanscom, S. R., McCaffrey, M. W., and Khan, A. R. (2013) Structural and functional analysis of FIP2 binding to the endosome-localised Rab25 GTPase. *Biochim. Biophys. Acta* **1834,** 2679–2690
31. Catz, S. D. (2013) Regulation of vesicular trafficking and leukocyte function by Rab27 GTPases and their effectors. *J. Leukocyte Biol.* **94,** 613–622
32. Cockcroft, S. (1991) Relationship between arachidonate release and exocytosis in permeabilized human neutrophils stimulated with formylmethionyl-leucyl-phenylalanine (fMetLeuPhe), guanosine 5′-[γ-thio]triphosphate (GTP[S]) and Ca2+. *Biochem. J.* **275**, 127–131
33. Brown, G. E., Stewart, M. Q., Bissonnette, S. A., Elia, A. E., Wilker, E., and Yaffe, M. B. (2004) Distinct ligand-dependent roles for p38 MAPK in priming and activation of the neutrophil NADPH oxidase. *J. Biol. Chem.* **279,** 27059–27068
34. Fan, G. H., Lapierre, L. A., Goldenring, J. R., Sai, J., and Richmond, A. (2004) Rab11-family interacting protein 2 and myosin Vb are required for CXCR2 recycling and receptor-mediated chemotaxis. *Mol. Biol. Cell* **15,** 2456–2469
35. Mudrakola, H. V., Zhang, K., and Cui, B. (2009) Optically resolving individual microtubules in live axons. *Structure* **17,** 1433–1441
36. Khandelwal, P., Ruiz, W. G., Balestreire-Hawryluk, E., Weisz, O. A., Goldenring, J. R., and Apodaca, G. (2008) Rab11a-dependent exocytosis of discoidal/fusiform vesicles in bladder umbrella cells. *Proc. Natl. Acad. Sci. U.S.A.* **105,** 15773–15778
37. Li, B. X., Satoh, A. K., and Ready, D. F. (2007) Myosin V, Rab11, and dRip11 direct apical secretion and cellular morphogenesis in developing *Drosophila* photoreceptors. *J. Cell Biol.* **177,** 659–669
38. Sugawara, K., Shibasaki, T., Mizoguchi, A., Saito, T., and Seino, S. (2009) Rab11 and its effector Rip11 participate in regulation of insulin granule exocytosis. *Genes Cells* **14,** 445–456
39. Su, T., Bryant, D. M., Luton, F., Vergés, M., Ulrich, S. M., Hansen, K. C., Datta, A., Eastburn, D. J., Burlingame, A. L., Shokat, K. M., and Mostov, K. E. (2010) A kinase cascade leading to Rab11-FIP5 controls transcytosis of the polymeric immunoglobulin receptor. *Nat. Cell Biol.* **12,** 1143–1153
40. Ren, Q., Wimmer, C., Chicka, M. C., Ye, S., Ren, Y., Hughson, F. M., and Whiteheart, S. W. (2010) Munc13-4 is a limiting factor in the pathway required for platelet granule release and hemostasis. *Blood* **116,** 869–877
41. Singh, R. K., Mizuno, K., Wasmeier, C., Wavre-Shapton, S. T., Recchi, C., Catz, S. D., Futter, C., Tolmachova, T., Hume, A. N., and Seabra, M. C. (2013) Distinct and opposing roles for Rab27a/Mlph/MyoVa and Rab27b/Munc13-4 in mast cell secretion. *FEBS J.* **280,** 892–903
42. Khandelwal, P., Prakasam, H. S., Clayton, D. R., Ruiz, W. G., Gallo, L. I., van Roekel, D., Lukianov, S., Peränen, J., Goldenring, J. R., and Apodaca, G. (2013) A Rab11a-Rab8a-Myo5B network promotes stretch-regulated exocytosis in bladder umbrella cells. *Mol. Biol. Cell* **24,** 1007–1019
43. Khvotchev, M. V., Ren, M., Takamori, S., Jahn, R., and Südhof, T. C. (2003) Divergent functions of neuronal Rab11b in Ca2+-regulated versus constitutive exocytosis. *J. Neurosci.* **23,** 10531–10539
44. Savina, A., Fader, C. M., Damiani, M. T., and Colombo, M. I. (2005) Rab11 promotes docking and fusion of multivesicular bodies in a calcium-dependent manner. *Traffic* **6,** 131–143
45. Yu, S., Nie, Y., Knowles, B., Sakamori, R., Stypulkowski, E., Patel, C., Das, S., Douard, V., Ferraris, R. P., Bonder, E. M., Goldenring, J. R., Ip, Y. T., and Gao, N. (2014) TLR sorting by Rab11 endosomes maintains intestinal epithelial-microbial homeostasis. *EMBO J.* **33,** 1882–1895